

Structure of the Pyrroloquinoline Quinone Radical in Quinoprotein Ethanol Dehydrogenase*

Received for publication, October 12, 2005 Published, JBC Papers in Press, November 2, 2005, DOI 10.1074/jbc.M511132200

Christopher W. M. Kay^{†1}, Bina Mennenga[§], Helmut Görisch[§], and Robert Bittl[‡]

From the [‡]Institut für Experimentalphysik, Fachbereich Physik, Freie Universität Berlin, 14195 Berlin, Germany and [§]Fachgebiet Technische Biochemie, Institut für Biotechnologie, Technische Universität Berlin, 13353 Berlin, Germany

Quinoprotein alcohol dehydrogenases use the pyrroloquinoline quinone (PQQ) cofactor to catalyze the oxidation of alcohols. The catalytic cycle is thought to involve a hydride transfer from the alcohol to the oxidized PQQ, resulting in the generation of aldehyde and reduced PQQ. Reoxidation of the cofactor by cytochrome proceeds in two sequential steps via the PQQ radical. We have used a combination of electron nuclear double resonance and density functional theory to show that the PQQ radical is not protonated at either O-4 or O-5, a result that is at variance with the general presumption of a singly protonated radical. The quantum mechanical calculations also show that reduced PQQ is unlikely to be protonated at O-5; rather, it is either singly protonated at O-4 or not protonated at either O-4 or O-5, a result that also challenges the common assumption of a reduced PQQ protonated at both O-4 and O-5. The reaction cycle of PQQ-dependent alcohol dehydrogenases is revised in light of these findings.

A number of Gram-negative bacteria utilize a class of dehydrogenases known as quinoproteins, which are distinct from the flavin- and nicotinamide-dependent enzymes, to catalyze the oxidation of alcohols or aldoses (1–3). The reaction is the first step in an electron transport chain that generates a proton motive force that is used to produce ATP. Several quinoproteins contain the noncovalently bound quinoid cofactor pyrroloquinoline quinone (PQQ)² (Fig. 1), the role of which as a potential vitamin in mammals is currently under debate (4–6). Among this class of enzymes, methanol dehydrogenase (MDH) (7–15), quinoprotein ethanol dehydrogenase (QEDH) (16), quinohepotein alcohol dehydrogenase (QH-ADH) (17, 18), and soluble glucose dehydrogenase (s-GDH) (19) have been described and crystallized. Spectroscopic, biochemical, and in particular x-ray crystallographic studies have allowed great progress to be made in the understanding of the structure and function of these proteins (20–22).

The most frequently investigated PQQ-dependent alcohol dehydrogenase is MDH. This soluble enzyme is a heterotetramer of two large and two small subunits ($\alpha_2\beta_2$) (8–12, 14, 15). In contrast, QEDH is composed of two large subunits (α_2) (16). The common structure of the α -subunit is a super-barrel composed of eight radially arranged

β -sheets, a so-called propeller fold. The PQQ cofactor bound to a Ca^{2+} ion is buried in the interior of the super-barrel and sandwiched between the indole ring of a tryptophan residue and an eight-member disulfide ring formed from adjacent cysteine residues. In QEDH these are Cys¹⁰⁵ and Cys¹⁰⁶ (16).

Two mechanisms have been proposed for the oxidation of alcohols in quinoprotein dehydrogenases, both of which begin with the PQQ in an oxidized state. Initially, an addition/elimination mechanism was proposed, a suggestion that is now considered unlikely; rather, a hydride transfer mechanism is preferred (19, 23, 24) (see Fig. 1). Following substrate binding, the reaction is initiated by amino acid (Asp (11) or Glu (25)) base-catalyzed proton abstraction of the hydroxyl proton of the alcohol. Nucleophilic attack of the hydride from the substrate to the C-5 position of PQQ then occurs. Subsequently, the PQQ enolizes to form the quinol. The reduced PQQ is reoxidized by two sequential single electron transfers (ET) to cytochrome c_L in MDH, cytochrome c_{550} in QEDH, or the cytochrome c domain in QH-ADH via the intermediate free radical (26–28), a process that is thought to be mediated by the disulfide bridge (17, 18, 29).

Information that is not usually obtained from x-ray analysis but is necessary for obtaining a full understanding of a dehydrogenation reaction cycle concerns the protonation states of the singly and doubly reduced species. As shown in Fig. 1, apart from one review (21), reduced PQQ is usually shown protonated at both O-4 and O-5, whereas the radical is depicted singly protonated at either O-4 (30, 31) or O-5 (20, 24, 32), although a deprotonated radical was recently postulated (33). Knowledge of the protonation states is crucial if the ET and proton transfer pathways in both reoxidation steps are to be understood, because depending on the protonation states of the initial and final molecules, the reaction is either simple ET or must be accompanied by the release of a proton. Furthermore, apart from the driving force and the reorganization energy, according to ET theory (34), the rate of ET is dependent on the electronic coupling between the donor (PQQ) and acceptor (heme). Therefore, a full understanding of ET kinetics in quinoproteins will only be possible with knowledge of both the spatial and electronic structures of the ET partners (35). The latter may be provided by electron nuclear double resonance (ENDOR) via determination of hyperfine couplings (hfc) in combination with density functional theory (DFT) calculations (36). These methods enable us to establish that the PQQ radical is deprotonated when bound in QEDH from *Pseudomonas aeruginosa*. In the light of this finding, we present here a revised reaction cycle for PQQ-dependent dehydrogenases.

MATERIALS AND METHODS

Enzyme Isolation—The apof orm of QEDH enzyme was heterologously over-expressed in *Escherichia coli* and purified to homogeneity as described earlier for holoQEDH (37, 38).

Reconstitution of the Holoform of QEDH—The formation of an enzymatically active holoenzyme in either protiated or deuteriated buffer

* This work was supported by the Deutsche Forschungsgemeinschaft (Sonderforschungsbereich 498, Teilprojekt C5, and Go 242/12-1). The costs of publication of this article were defrayed in part by the payment of page charges. This article must therefore be hereby marked "advertisement" in accordance with 18 U.S.C. Section 1734 solely to indicate this fact.

¹ To whom correspondence should be addressed: Institut für Experimentalphysik, Fachbereich Physik, Freie Universität Berlin, Arnimallee 14, 14195 Berlin, Germany. Tel.: 49-30-8385-3394; Fax: 49-30-8385-6046; E-mail: chris.kay@physik.fu-berlin.de.

² The abbreviations used are: PQQ, pyrroloquinoline quinone; MDH, methanol dehydrogenase; QEDH, quinoprotein ethanol dehydrogenase; QH-ADH, quinohepotein alcohol dehydrogenase; s-GDH, soluble-glucose dehydrogenase; ENDOR, electron nuclear double resonance; hfc, hyperfine coupling; HOMO, highest occupied molecular orbital; LUMO, lowest occupied molecular orbital; SOMO, singly occupied molecular orbital; ET, electron transfer; DFT, density functional theory.

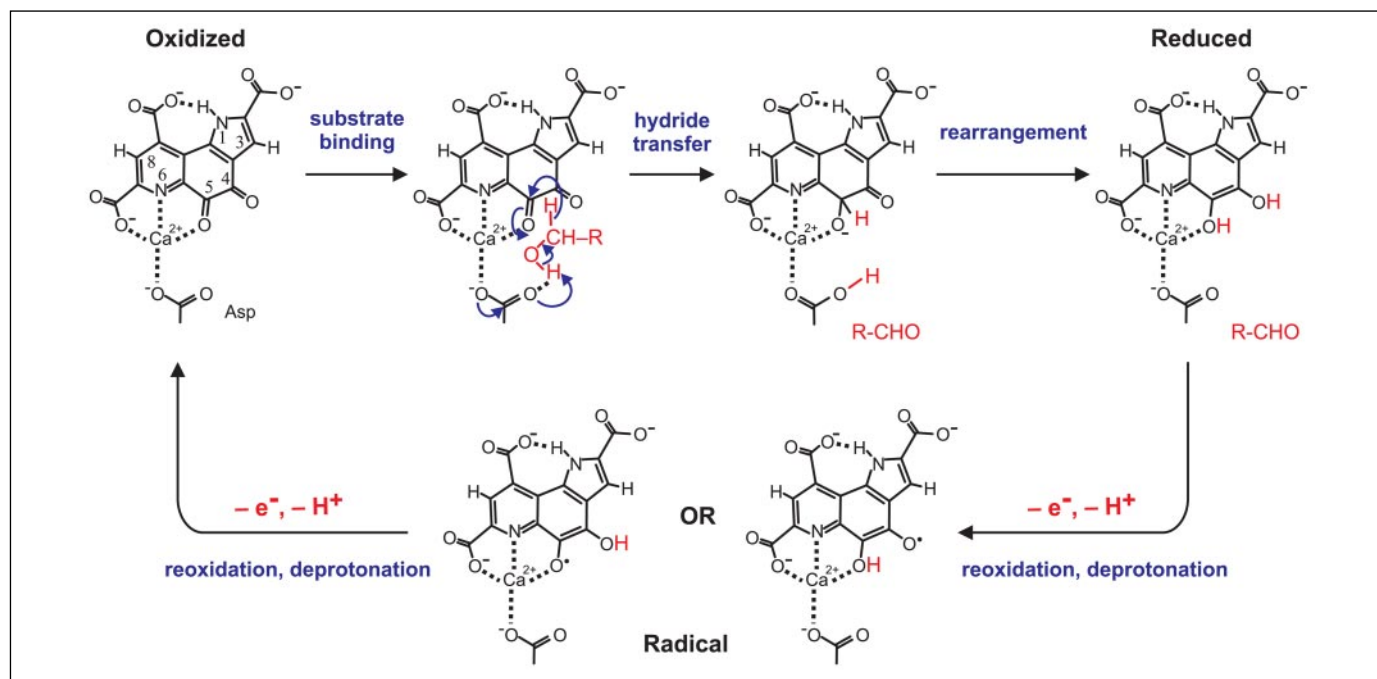


FIGURE 1. The currently accepted reaction cycle for alcohol oxidation in quinoproteins, adapted from Anthony and Williams (24). The mechanism is based on a hydride transfer from the alcohol to the C-5 position of the PQQ (19). The back-reaction is via a radical intermediate protonated at O-4 or O-5. The IUPAC numbering scheme of PQQ is also shown.

was achieved as described previously (39). Before reconstitution, the enzyme was transferred to the appropriate buffer (protiated or deuteriated) by ultrafiltration using Centricon filters with a 30-kDa cut-off (Millipore, Billerica, MA). PQQ (Sigma) was dissolved in the same buffer.

In a previous study we observed that following reconstitution or isolation of the native enzyme, substrate is often bound (40). Therefore, following reconstitution the preparations were washed by repeated ultrafiltration cycles in freshly prepared alcohol-free protiated or deuteriated buffer (100 mM Tris/HCl, 100 mM NaCl, 10 mM CaCl₂). Finally, the samples were concentrated to a subunit concentration of 300 μ M.

EPR Sample Preparation—The enzyme preparations were transferred into 3-mm (inner diameter) quartz tubes for X-band (9 GHz) EPR and 0.7-mm (inner diameter) quartz tubes for W-band (94 GHz) EPR.

EPR Instrumentation—X-band continuous wave EPR spectra were recorded using a pulsed EPR spectrometer (Bruker Elexsys E580) equipped with an EPR resonator (SHQEW0401) cooled by a helium cryostat (Oxford ESR 910).

X-band-pulsed ENDOR spectra were recorded using the same spectrometer together with a DICE-ENDOR accessory including a radiofrequency amplifier (Amplifier Research 250A250A) and a dielectric ring ENDOR resonator (Bruker EN4118X-MD-4-W1), which was immersed in a helium gas flow cryostat (Oxford CF-935). For Davies-type ENDOR, a microwave pulse sequence π - t - $\pi/2$ - τ - π using 64- and 128-ns $\pi/2$ and π pulses, respectively, and a radiofrequency pulse of 10 μ s duration, starting 1 μ s after the first microwave pulse, were used. The separation times t and τ between the microwave pulses were selected to be 13 μ s and 500 ns, respectively.

W-band-pulsed ENDOR spectra were recorded using a pulsed EPR spectrometer (Bruker Elexsys E680) equipped with a DICE-ENDOR accessory including a radiofrequency amplifier (Amplifier Research 250A250A) and an ENDOR resonator (Bruker Teraflex EN600-1021H), which was immersed in a helium gas flow cryostat (Oxford). For Davies-type ENDOR, a microwave pulse sequence π - t - $\pi/2$ - τ - π

using 120- and 240-ns $\pi/2$ and π pulses, respectively, and an RF pulse of 20 μ s duration, starting 1 μ s after the first microwave pulse, were used. The separation times t and τ between the microwave pulses were selected to be 25 μ s and 600 ns, respectively.

All experiments were performed at 80 K. The pulse patterns were repeated with a frequency of 200 Hz so as to avoid saturation effects due to long relaxation times. Note that as no modulation was used, the ENDOR spectra are in absorption. To increase signal-to-noise and to aid interpretation and discussion, the ENDOR spectra have been symmetrized with respect to the nuclear Zeeman frequency. They are displayed on an hfc axis centered at the nuclear Zeeman frequency.

Computations—DFT was used to calculate the geometric and electronic structure of PQQ in several oxidation and protonation states. Geometries were optimized at the B3LYP/6-311G(*d,p*) level of theory, as implemented in the program package Gaussian 03 (41). For closed shell and radical species, restricted and unrestricted calculations, respectively, were performed. Single point calculations of isotropic and dipolar hfc's were carried out on the optimized geometries. Graphical representations of molecular orbitals and electron spin density surfaces were achieved using the Molden program package (42) followed by rendering with POV-RayTM.

RESULTS AND DISCUSSION

EPR—The X-band cw-EPR spectrum of the PQQ radical bound in QEDH is shown in Fig. 2 (*continuous line*). The spectrum shows a slightly asymmetric line shape centered at $g_{\text{iso}} = 2.0043$ and a peak-to-peak line width of 0.5 millitesla and is similar to that observed in MDH (3, 43, 44), s-GDH (33), and QH-EDH (45). Typical of all of the EPR spectra is the shoulder at low field and the ease of microwave saturation. When the enzyme was reconstituted in deuteriated buffer, the peak-to-peak line width was reduced only slightly, but the shoulders decreased in relative intensity (Fig. 2, *dotted line*). The narrow line width of both spectra and the absence of dramatic changes when comparing the two samples are qualitative evidence that the exchangeable protons have

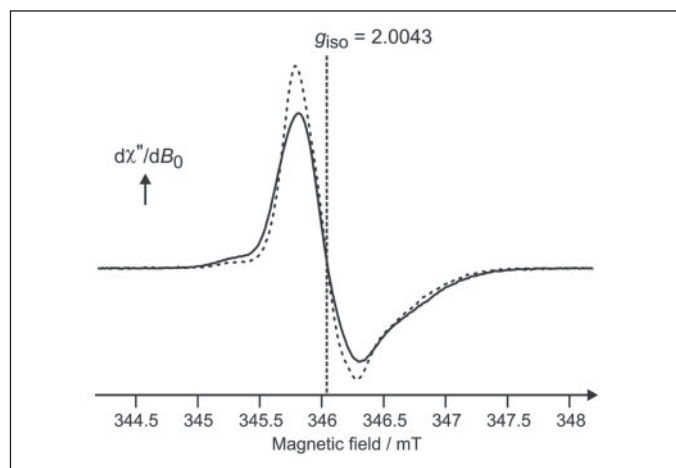


FIGURE 2. Continuous wave EPR spectra of the PQQ radical bound in QEDH. Enzyme was reconstituted in H₂O buffer (solid line) and in D₂O buffer (dotted line). The spectra have been normalized to have the same double integral. Experimental conditions: microwave frequency, 9.384 GHz; microwave power, 2 microwatts; magnetic field modulation amplitude, 0.1 millitesla (frequency 100 kHz).

only small hfc. Hence, to garner more specific details about the protonation state of the PQQ radical, we have turned to the higher resolution of ENDOR.

ENDOR—X-band-pulsed ENDOR spectra of the PQQ radical bound in QEDH and reconstituted in protiated buffer and deuteriated buffer are displayed in Fig. 3, A and B, respectively. The ENDOR spectra are centered at the nuclear Zeeman frequency ($\nu_H = 14.75$ MHz), and in the weak coupling limit, which is the case here, each set of equivalent protons gives rise to a pair of tensorial patterns, whereby the splitting is equal to the hfc component (Fig. 3A). To aid comparison, the spectra have been normalized so that the outer shoulder and peak (in the range of $\nu_H \pm 6$ to 10 MHz), which appear to be almost unaffected by changes in the buffer, have the same intensity.

The spectrum from QEDH reconstituted in protiated buffer exhibits a very rich and well resolved hyperfine structure with hfc's in the range of 0 to 10 MHz. When the enzyme was reconstituted in deuteriated buffer, there was a dramatic reduction in intensity in the middle part of the spectrum. The difference between the spectra recorded in deuteriated buffer and protiated buffer is shown in Fig. 3C. The difference spectrum gives us a high degree of confidence that the exchangeable protons have hfc's in the range of 0 to 5 MHz, one of which is expected to be the proton at N-1. The protonation states of the three carboxylic acid groups of PQQ when bound in quinoproteins are not known, although in solution at pH 7 it is expected that they would be deprotonated (33, 46). Nevertheless, even if they were protonated, such protons always have negligible hfc's. The only other positions in the cofactor that could have exchangeable protons with significant hfc's are at O-4 and O-5. Other contributions can arise from exchangeable protons such as water molecules, in the binding pocket, and nearby amino acids such as Arg³⁴⁴.

The spectrum from the sample reconstituted in deuteriated buffer (Fig. 3B) should contain only nonexchangeable protons, of which the PQQ cofactor has two, at C-3 and C-8. Indeed, outside of the matrix region (>2 MHz), two tensorial patterns are discernable. One has rhombic symmetry and components at 9.6 and 6.2 MHz, whereas the third and smallest component is smaller and hidden. The second has a narrow and intense component at 4.0 MHz, which implies axial symmetry, although the other component cannot be positively identified. The matrix region (<2 MHz) shows an intense signal and some structure, but it cannot be easily interpreted. We expect that it is due in part

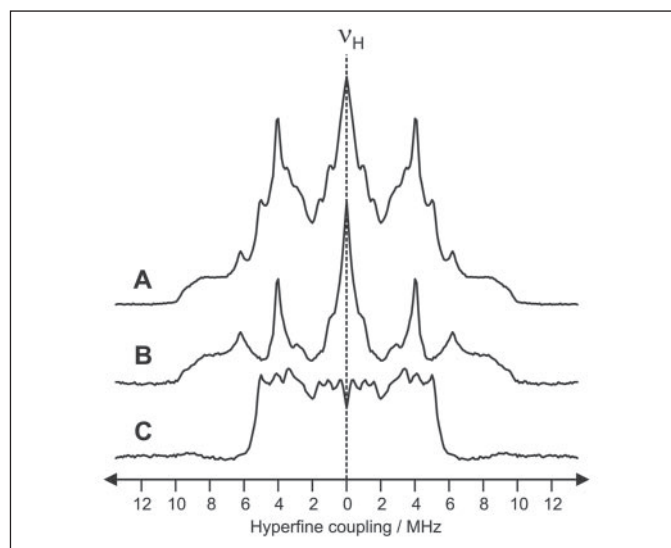


FIGURE 3. X-band-pulsed ENDOR spectra of the PQQ radical bound in QEDH. Enzyme was reconstituted in H₂O buffer (A) and in D₂O buffer (B). C, difference between the two spectra shown in A and B.

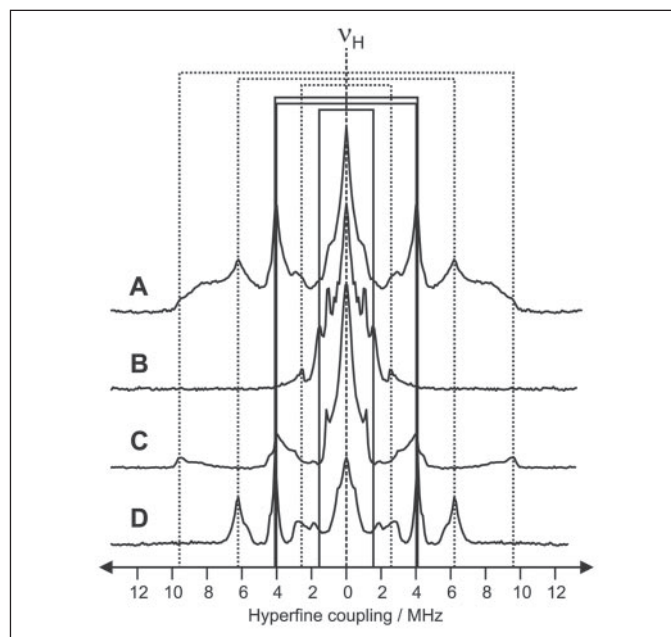


FIGURE 4. Pulsed ENDOR spectra of the PQQ radical bound in QEDH reconstituted in D₂O at X-band (A) and at W-band (B–D). B–D, spectra were recorded at field positions corresponding to molecules with their axes parallel to the external magnetic field: B, g_x ; C, g_y ; D, g_z . Also shown are two pairs of three lines corresponding to the three principal components of the two hyperfine tensors discussed in the text.

to the β -protons on the cysteine residues forming a disulfide bridge that is in van der Waals contact with the PQQ cofactor.

To gain a more complete understanding of the spectrum containing only nonexchangeable protons, we performed pulsed ENDOR experiments at W-band. The improved spectral resolution provided by the increased Zeeman interaction allows us to measure ENDOR spectra with orientation selection. Fig. 4 shows the X-band ENDOR spectrum (A) together with the W-band spectra (B, C, and D) of the same sample recorded at magnetic field positions in the W-band EPR spectrum at which principal values of the g -tensor are on resonance. The W-band EPR spectrum and principal values of the g -tensor have been published previously and are not repeated here (40).

TABLE 1

Comparison of experimental and calculated proton hfcs for the PQQ radical bound in QEDH

All values are in MHz. The experimental values have errors of ± 0.05 MHz. The signs are given by comparison with the theoretical values. For the protons at positions C-3 and C-8, the experimental values are given as A_{xx} , A_{yy} , and A_{zz} , as these may be assigned by the W-band ENDOR experiments. For the exchangeable proton at N-1 and the putative protons at positions O-4 and O-5, there is no directional assignment, and they are simply labeled as A_1 , A_2 , and A_3 .

Proton	Experimental values for QEDH from <i>P. aeruginosa</i>	Calculated values		
		Anion radical $\text{Ca}^{2+}\text{PQQ}^{4\cdot-}$	Neutral radical $\text{Ca}^{2+}\text{PQQ}(4)\text{H}^{3\cdot-}$	Neutral radical $\text{Ca}^{2+}\text{PQQ}(5)\text{H}^{3\cdot-}$
N-1				
A_1	<5	-4.88	-3.21	-1.50
A_2	<5	-4.13	-1.80	0.34
A_3	<5	0.24	3.17	0.99
C-3				
A_{yy}	(-)4.1	-3.62	-1.35	-24.12
A_{zz}	(-)4.0	-3.55	0.92	-18.10
A_{xx}	(-)1.6	-1.01	1.99	-5.18
O-4				
A_1			-3.17	
A_2			-2.08	
A_3			1.55	
O-5				
A_1				-1.68
A_2				-0.73
A_3				0.60
C-8				
A_{yy}	(-)9.6	-11.11	-5.35	-1.07
A_{zz}	(-)6.2	-7.06	-3.78	-0.15
A_{xx}	(-)2.6	-1.63	-0.73	1.10

The advantage of W-band ENDOR over conventional X-band ENDOR is immediately apparent. The powder-type X-band spectrum is separated into three more simple spectra. The most straightforward ENDOR spectrum to interpret is that with the magnetic field parallel to g_z (Fig. 4D). Given that the PQQ cofactor is approximately planar, an assumption that all x-ray data and quantum mechanical calculations support, then as in all quinoids, g_z is expected to be perpendicular to the molecular frame. Hence, only molecules with their planes perpendicular to the external magnetic field are on resonance at this position. Therefore, only the component of the hfc tensor that is perpendicular to the molecular plane is detected. For the C-3 and C-8 α -protons of PQQ, this is the middle hfc component, and indeed, the spectrum recorded at g_z shows two intense transitions, with hfcs A_{zz} of 6.2 and 4.0 MHz, which are also observed at X-band.

The spectrum recorded at g_y (Fig. 4C) also shows two distinct, albeit broader transitions: a large hfc with a maximum at 9.6 MHz and a smaller hfc of 4.1 MHz. Again, these can be associated directly with the equivalent transitions in the X-band spectrum. In the spectrum taken at g_x (Fig. 4B), all large hfcs have vanished and only a single pair of lines with a hfc of 2.6 MHz is observed outside the intense matrix region. On the flanks of the matrix region is another pair of lines with a hfc of 1.6 MHz.

Taking all this information together, we obtain, for two nonexchangeable protons, one symmetric rhombic tensor with components $A_{xx} = 2.6$ MHz, $A_{yy} = 9.6$ MHz, $A_{zz} = 6.2$ MHz and one almost axial tensor with components $A_{xx} = 1.6$ MHz, $A_{yy} = 4.1$ MHz, $A_{zz} = 4.0$ MHz. The experimental values are collected in Table 1. In previous Q-band ENDOR studies on MDH, the two quite similar A_{zz} components were determined: $A_{zz,1} = 6.6$ MHz and $A_{zz,2} = 4.1$ MHz in *Rhodospseudomonas acidophila* (47) and $A_{zz,1} = 6.3$ MHz and $A_{zz,2} = 3.7$ MHz in *Hyphomicrobium X* (43). The comparison shows that the electronic structure of the PQQ radical in MDH and QEDH is quite similar, so that we expect that the results obtained here should be generally applicable to this class of enzymes.

Quantum Mechanical Calculations—To assign the hfcs we carried out DFT calculations on the PQQ radical. The ground state oxidized

PQQ was taken as $\text{PQQ}^{3\cdot-}$ with all three carboxyl groups deprotonated in line with spectroelectrochemical studies (33, 46), an approach that has been included in recent quantum chemical calculations (48, 49). Hence, formally the one-electron reduced PQQ radical has the structure $\text{PQQ}^{4\cdot-}$.

Previous quantum mechanical calculations have shown that the binding of Ca^{2+} has very little effect on the geometry of PQQ (30). Nevertheless, as it is present in all quinoproteins, it was also included here giving $\text{Ca}^{2+}\text{PQQ}^{4\cdot-}$ as the *anion* radical form. The literature portrays two possible *neutral* radical forms, $\text{Ca}^{2+}\text{PQQH}^{3\cdot-}$ with the PQQ protonated at either O-4, $\text{Ca}^{2+}\text{PQQ}(4)\text{H}^{3\cdot-}$, or O-5, $\text{Ca}^{2+}\text{PQQ}(5)\text{H}^{3\cdot-}$ (see Fig. 1). We take the anion and neutral nomenclature from the flavin literature. The predicted hfc parameters for the protons are collected in Table 1.

All three structures converged, and apart from the carboxylic group at C-9, which was slightly twisted to form a better hydrogen bond with the proton at N-1, the geometries were approximately planar, in agreement with previous work (30, 48). However, it is not our purpose here to discuss all the details of the structures; rather we have concentrated on comparing the experimental and theoretical hfcs.

$\text{Ca}^{2+}\text{PQQ}(4)\text{H}^{3\cdot-}$ and $\text{Ca}^{2+}\text{PQQ}(5)\text{H}^{3\cdot-}$ are structural isomers, and therefore we can compare their energies directly. The total energy of $\text{Ca}^{2+}\text{PQQ}(5)\text{H}^{3\cdot-}$ is 71 kJ mol⁻¹ more unfavorable than $\text{Ca}^{2+}\text{PQQ}(4)\text{H}^{3\cdot-}$. The coordinate bond from O-H to Ca^{2+} is clearly weaker than that from O⁻ to Ca^{2+} . The hfcs of $\text{Ca}^{2+}\text{PQQ}(4)\text{H}^{3\cdot-}$ are all small, whereas $\text{Ca}^{2+}\text{PQQ}(5)\text{H}^{3\cdot-}$ has one very large hfc for the proton at C-3. The hfcs of neither isomer match the experimental data.

The calculations for $\text{Ca}^{2+}\text{PQQ}^{4\cdot-}$ predict two medium-sized hfcs for the nonexchangeable protons. The tensor of the proton bound at C-8 is larger and has a rhombic shape, whereas that at C-3 is smaller and axial. The magnitudes and symmetries match the experimental data rather well (see Table 1). Furthermore, the hfc tensor components for the proton at N-1 are all under 5 MHz, which is what we expected from the H₂O/D₂O buffer exchange experiments. Similar results were obtained from calculations in which all three carboxylic acid groups were protonated (not shown). The good agreement between theory and experi-

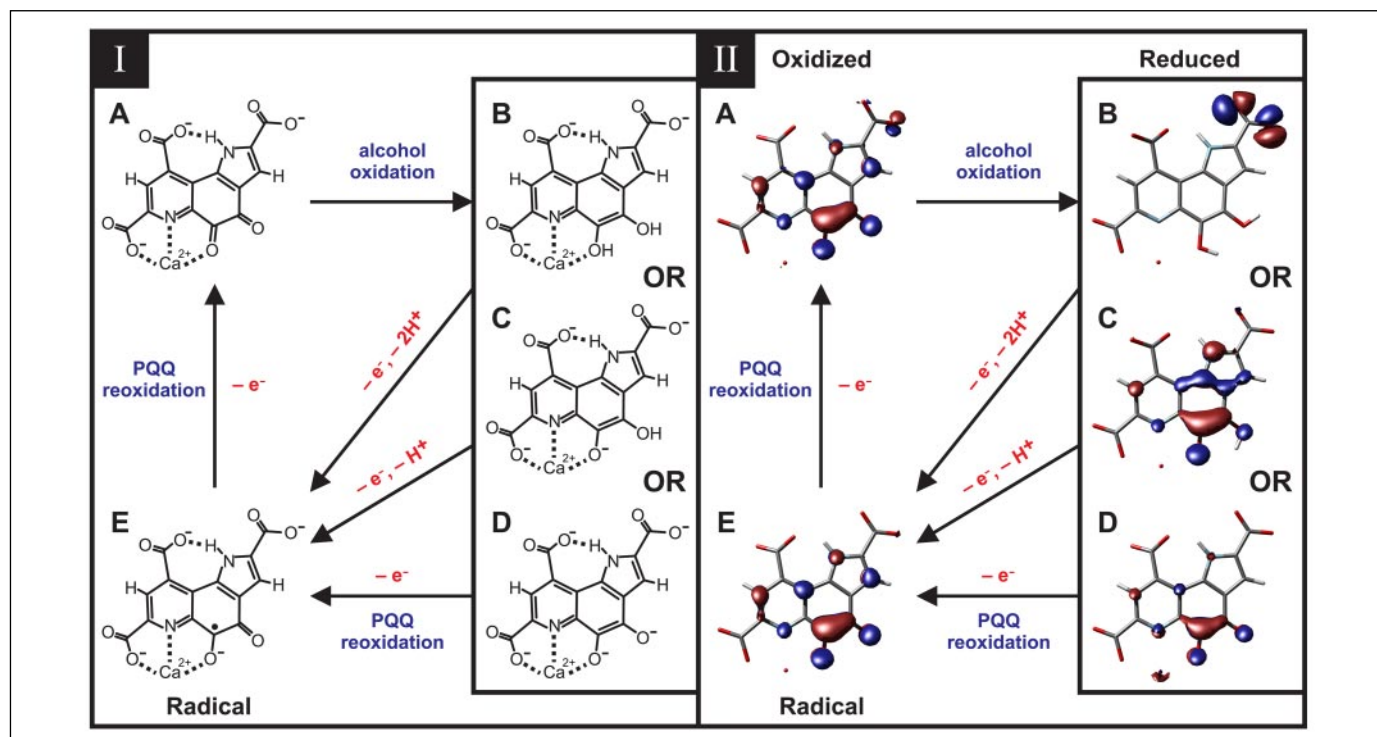


FIGURE 5. Revised reaction cycle for PQQ-dependent quinoproteins showing the molecular structures (I) and the molecular orbitals (II) of intermediates that are known to be present (A and E) or potentially present (B, C, and D). Oxidized PQQ (A) is reduced by hydride transfer from the alcohol, resulting in the formation of a reduced PQQ in one of three possible protonation states: B, doubly protonated, $\text{Ca}^{2+}\text{PQQH}_2^{3-}$; C, singly protonated, $\text{Ca}^{2+}\text{PQQH}^{4-}$; or D, deprotonated, $\text{Ca}^{2+}\text{PQQ}^{5-}$. The reoxidation of the reduced PQQ is achieved by two sequential ET steps to cytochrome via the deprotonated $\text{Ca}^{2+}\text{PQQ}^{4\cdot-}$ radical complex (E). The molecular orbitals are presented at a contour level of $0.05 \text{ e}/\text{au}^3$. The blue and red areas denote regions of opposite signs of the wave function.

ment establishes that the PQQ radical in QEDH is deprotonated at O-4 and O-5, as was recently suggested for the PQQ radical in s-GDH (33).

To summarize, we have shown that the PQQ radical in QEDH is well described by a $\text{Ca}^{2+}\text{PQQ}^{4\cdot-}$ complex and now will consider the implications of this result for the reaction mechanism (Fig. 5). Panel I (Fig. 5) shows the molecular structures that are active or potentially active in each step, and panel II shows the molecular orbitals of these species. The oxidation of the radical species (Fig. 5E) $\text{Ca}^{2+}\text{PQQ}^{4\cdot-}$ to the oxidized species (Fig. 5A) $\text{Ca}^{2+}\text{PQQ}^{3-}$ is a simple ET to cytochrome. The singly occupied molecular orbital (SOMO) for the $\text{Ca}^{2+}\text{PQQ}^{4\cdot-}$ complex derived from DFT calculations is presented in Fig. 5E, panel II. It has a highly localized electron density concentrated on the central ring with a maximum at C-5 and appears designed to have optimal overlap with the orbitals of the sulfur of the nearby Cys¹⁰⁶ (4 Å above C-5), thus promoting electron transfer to the electron acceptor via the disulfide bridge.

We optimized the structure of the oxidized species, $\text{Ca}^{2+}\text{PQQ}^{3-}$, and have displayed the lowest unoccupied molecular orbital (LUMO) in Fig. 5A, panel II. The loss of one electron in comparison with the radical species has only a small effect on the electronic structure. The minor changes to the orbital imply that there will be only minimal electronic reorganization accompanying the ET, thus enhancing the rate.

Furthermore, the LUMO of the oxidized PQQ has the proper form, maximum electron density at C-5, to act as hydride acceptor during alcohol oxidation. Following this reaction, reduced PQQ is formed. The protonation state of this species when bound in the protein is not known, although it is usually depicted as the quinol, PQQH_2 , protonated at both O-4 and O-5. Nevertheless, there does not seem to be any reason why the two protons liberated during the oxidation of ethanol should not be immediately released (see Fig. 1). This is particularly true for the proton abstracted from the alcohol by the amino acid base, Asp or Glu, which does not have to be transferred to the PQQ. On the other

hand, the intermediate PQQ species formed by hydride addition to C-5 does provide a proton that could relocate to O-4 by enolization. Indeed, Arg³⁴⁴, which is located close to O-4 and O-5, provides a positive charge that could balance a negatively charged reduced PQQ. For comparison, a negatively charged reduced form is common in flavoproteins, *i.e.* FADH^- .

This reasoning led us to perform DFT calculations on the possible protonation states of the reduced species shown in Fig. 5: protonated at both O-4 and O-5, $\text{Ca}^{2+}\text{PQQH}_2^{3-}$ (B); singly protonated at O-4 or O-5, $\text{Ca}^{2+}\text{PQQH}^{4-}$ (C); deprotonated, $\text{Ca}^{2+}\text{PQQ}^{5-}$ (D). The step to form the radical $\text{Ca}^{2+}\text{PQQ}^{4\cdot-}$ (Fig. 5E) depends on the nature of the reduced species. The simplest reaction would be a straightforward ET from $\text{Ca}^{2+}\text{PQQ}^{5-}$ to cytochrome. If we start out from $\text{Ca}^{2+}\text{PQQH}^{4-}$, then the ET must be accompanied by the loss of a proton, and from $\text{Ca}^{2+}\text{PQQH}_2^{3-}$ by the loss of two protons.

We have optimized the geometry of the deprotonated reduced species, $\text{Ca}^{2+}\text{PQQ}^{5-}$, and display the highest occupied molecular orbital (HOMO) in Fig. 5D. The addition of one electron to the radical species has some effect on the orbital with a markedly reduced electron density on N-1 and C-3. Nevertheless, it still has a high electron density at C-5 close to the cysteinyl sulfur for optimal orbital overlap and efficient ET to cytochrome, and thus this structure is a good candidate for the reduced species.

ET concomitant with proton release to generate the $\text{Ca}^{2+}\text{PQQ}^{4\cdot-}$ radical from the reduced $\text{Ca}^{2+}\text{PQQH}^{4-}$ is certainly possible, but again it is important to know the electron density distribution in the HOMO. Hence, we have optimized the geometries of the two isomers. As in the radical, the protonation of O-5 appears to be very unfavorable, and the species protonated at O-4 is 84 kJ mol^{-1} more stable. The HOMO of this species is displayed in Fig. 5C. Its electron density distribution is also quite similar to that of the radical $\text{Ca}^{2+}\text{PQQ}^{4\cdot-}$ (Fig. 5E), with good

overlap with the disulfide bridge, and therefore this structure is also a good candidate for the reduced species.

Given the high energetic cost of protonating the reduced species at O-5, it seems implausible that a doubly protonated $\text{Ca}^{2+}\text{PQQH}_2^{3-}$ (Fig. 5B) would be an active intermediate. Furthermore, formation of the $\text{Ca}^{2+}\text{PQQ}^{4-}$ radical from $\text{Ca}^{2+}\text{PQQH}_2^{3-}$ by ET accompanied by the loss of two protons also appears unlikely, but as it is the standard structure given in the literature we also considered this possibility. We have optimized the structure and display the HOMO in Fig. 5B, panel II. The protonation of O-5 has a dramatic effect, in that the HOMO now has almost no electron density on the central ring; rather, this is concentrated on the carboxylic group at C-2. The orbital overlap with the disulfide bridge is now very much lower, so that a reduced species with this structure would not be expected to be a good electron donor via the disulfide bridge pathway. Furthermore, the electronic reorganization following ET is now significant, which can only diminish the rate.

The clear finding is that in the reduced species O-5 is not protonated. Rather, this species is either deprotonated (Fig. 5D) or, in concurrence with one review article (21) and our chemical intuition, is singly protonated at O-4 (Fig. 5C). We favor the latter proposition, not only because this species is less highly charged but also because, in this case, the two protons liberated during the reaction cycle are released sequentially and not simultaneously. The first proton is released by the Asp or Glu during alcohol oxidation. This negates the need for the complex schemes often introduced to bring the proton abstracted by the amino acid base onto the PQQ. The second proton is released during the first step of PQQ reoxidation. The advantage of this scheme is that the proton flux produced by the enzyme is distributed over both halves of the reaction cycle.

Conclusions—hfcs calculated with DFT for a deprotonated radical complexed with a calcium ion, formally $\text{Ca}^{2+}\text{PQQ}^{4-}$ (Fig. 5E), are in good agreement with the experimental values. This agreement led us to present a model for the SOMO of the radical species that has highest electron densities at O-4, C-5, and O-5 on the central ring. This result is a beautiful example of the theory of orbital steering (50), as this orbital in its guises as SOMO (in the radical form) and LUMO (in oxidized form) has optimal spatial form to function in twin roles, as acceptor for a hydride transfer from substrate and as electron donor with good overlap with the orbitals of the disulfide bridge, thus promoting ET to cytochrome and reoxidation of the PQQ. Hence, these results support the proposed hydride transfer mechanism and an ET pathway via the disulfide bridge. For the reduced PQQ, energetics and the character of the HOMO clearly indicate that O-5 is deprotonated. We suggest that reduced PQQ is singly protonated at O-4 (Fig. 5C), although a doubly deprotonated species (Fig. 5D) cannot be entirely excluded.

Although the EPR spectrum of the PQQ radical bound in MDH was first observed many years ago (3), its nature has only now been correctly determined, and in the meantime the wrong structure has been used as a basis for mechanistic discussions. The actual structure of the PQQ radical bound in a quinoprotein and our suggestion for the structure of the reduced PQQ species provide a corrected reaction scheme in which electron and proton transfer pathways may be examined meaningfully. We hope that this contribution will encourage the use of the appropriate spectroscopic and theoretical techniques alongside x-ray crystallography to elucidate reaction mechanisms in full. The results are a salutary reminder that although protons are not usually observed in x-ray structures, they should not be neglected, as together with electrons, they are the moving parts of the enzymatic machine.

REFERENCES

- Hauge, J. G. (1964) *J. Biol. Chem.* **239**, 3630–3639
- Anthony, C., and Zatman, L. J. (1967) *Biochem. J.* **104**, 960–969
- Duine, J. A., Frank, J., and Westerling, J. (1978) *Biochim. Biophys. Acta* **524**, 277–287
- Kasahara, T., and Kato, T. (2003) *Nature* **422**, 832
- Felton, L. M., and Anthony, C. (2005) *Nature* **433**, E10–E12
- Rucker, R., Storms, D., Sheets, A., Tchapanian, E., and Fascetti, A. (2005) *Nature* **433**, E10–E12
- Xia, Z.-X., Dai, W.-W., Xiong, J. P., Hao, Z. P., Davidson, V. L., White, S., and Mathews, F. S. (1992) *J. Biol. Chem.* **267**, 22289–22297
- Xia, Z.-X., Dai, W.-W., Zhang, Y.-F., White, S. A., Boyd, G. D., and Mathews, F. S. (1996) *J. Mol. Biol.* **259**, 480–501
- Xia, Z.-X., He, Y.-N., Dai, W.-W., White, S. A., Boyd, G. D., and Mathews, F. S. (1999) *Biochemistry* **38**, 1214–1220
- Zheng, Y.-J., Xia, Z.-X., Chen, Z.-W., Mathews, F. S., and Bruce, T. C. (2001) *Proc. Natl. Acad. Sci. U. S. A.* **98**, 432–434
- Afolabi, P. R., Mohammed, F., Amaratunga, K., Majekodunmi, O., Dales, S. L., Gill, R., Thompson, D., Cooper, J. B., Wood, S. P., Goodwin, P. M., and Anthony, C. (2001) *Biochemistry* **40**, 9799–9809
- Williams, P. A., Coates, L., Mohammed, F., Gill, R., Erskine, P. T., Coker, A., Wood, S. P., Anthony, C., and Cooper, J. B. (2005) *Acta Crystallogr. Sect. D Biol. Crystallogr.* **61**, 75–79
- White, S., Boyd, G., Mathews, F. S., Xia, Z. X., Dai, W. W., Zhang, Y. F., and Davidson, V. L. (1993) *Biochemistry* **32**, 12955–12958
- Blake, C. C., Ghosh, M., Harlos, K., Avezoux, A., and Anthony, C. (1994) *Nat. Struct. Biol.* **1**, 102–105
- Ghosh, M., Anthony, C., Harlos, K., Goodwin, M. G., and Blake, C. (1995) *Structure (Lond.)* **3**, 177–187
- Keitel, T., Diehl, A., Knaute, T., Stezowski, J. J., Höhne, W., and Görisch, H. (2000) *J. Mol. Biol.* **297**, 961–974
- Oubrie, A., Rozeboom, H. J., Kalk, K. H., Huizinga, E. G., and Dijkstra, B. W. (2002) *J. Biol. Chem.* **277**, 3727–3732
- Chen, Z.-W., Matsushita, K., Yamashita, T., Fujii, T.-A., Toyama, H., Adachi, O., Bellamy, H. D., and Mathews, F. S. (2002) *Structure (Lond.)* **10**, 837–849
- Oubrie, A., Rozeboom, H. J., Kalk, K. H., Olsthoorn, A. J., Duine, J. A., and Dijkstra, B. W. (1999) *EMBO J.* **18**, 5187–5194
- Anthony, C. (1996) *Biochem. J.* **320**, 697–711
- Duine, J. A. (1999) *J. Biosci. Bioeng.* **88**, 231–236
- Anthony, C. (2004) *Arch Biochem. Biophys.* **428**, 2–9
- Oubrie, A., and Dijkstra, B. W. (2000) *Protein Sci.* **9**, 1265–1273
- Anthony, C., and Williams, P. (2003) *Biochim. Biophys. Acta* **1647**, 18–23
- Reddy, S. Y., and Bruce, T. C. (2003) *J. Am. Chem. Soc.* **125**, 8141–8150
- Duine, J. A., and Frank, J. (1980) *Biochem. J.* **187**, 221–226
- Frank, J., Dijkstra, M., Duine, J. A., and Balny, C. (1988) *Eur. J. Biochem.* **174**, 331–338
- Dijkstra, M., Frank, J., and Duine, J. A. (1989) *Biochem. J.* **257**, 87–94
- Avezoux, A., Goodwin, M. G., and Anthony, C. (1995) *Biochem. J.* **307**, 735–741
- Zheng, Y.-J., and Bruce, T. C. (1997) *Proc. Natl. Acad. Sci. U. S. A.* **94**, 11881–11886
- Duine, J. A., Frank, J., and De Beer, R. (1984) *Arch Biochem. Biophys.* **233**, 708–711
- Oubrie, A. (2003) *Biochim. Biophys. Acta* **1647**, 143–151
- Sato, A., Takagi, K., Kano, K., Kato, N., Duine, J. A., and Ikeda, T. (2001) *Biochem. J.* **357**, 893–898
- Marcus, R. A., and Sutin, N. (1985) *Biochim. Biophys. Acta* **811**, 265–322
- Davidson, V. L. (2004) *Arch Biochem. Biophys.* **428**, 32–40
- Büttner, T., Geier, J., Frison, G., Harmer, J., Calle, C., Schweiger, A., Schonberg, H., and Grützmaker, H. (2005) *Science* **307**, 235–238
- Rupp, M., and Görisch, H. (1988) *Biol. Chem. Hoppe-Seyler* **369**, 431–439
- Kay, C. W. M., Mennenga, B., Görisch, H., and Bittl, R. (2004) *FEBS Lett.* **564**, 69–72
- Mutzel, A., and Görisch, H. (1991) *Agric. Biol. Chem.* **55**, 1721–1726
- Kay, C. W. M., Mennenga, B., Görisch, H., and Bittl, R. (2005) *J. Am. Chem. Soc.* **127**, 7974–7975
- Frisch, M. J., Trucks, G. W., Schlegel, H. B., Scuseria, G. E., Robb, M. A., Cheeseman, J. R., Montgomery, J. A., Vreven, T., Kudin, K. N., Burant, J. C., Millam, J. M., Iyengar, S. S., Tomasi, J., Barone, V., Mennucci, B., Cossi, M., Scalmani, G., Rega, N., Petersson, G. A., Nakatsuji, H., Hada, M., Ehara, M., Toyota, K., Fukuda, R., Hasegawa, J., Ishida, M., Nakajima, T., Honda, Y., Kitao, O., Nakai, H., Klene, M., Li, X., Knox, J. E., Hratchian, H. P., Cross, J. B., Bakken, V., Adamo, C., Jaramillo, J., Gomperts, R., Stratmann, R. E., Yazyev, O., Austin, A. J., Cammi, R., Pomelli, C., Ochterski, J. W., Ayala, P. Y., Morokuma, K., Voth, G. A., Salvador, P., Dannenberg, J. J., Zakrzewski, V. G., Dapprich, S., Daniels, A. D., Strain, M. C., Farkas, O., Malick, D. K., Rabuck, A. D., Raghavachari, K., Foresman, J. B., Ortiz, J. V., Cui, Q., Baboul, A. G., Clifford, S., Cioslowski, J., Stefanov, B. B., Liu, G., Liashenko, A., Piskorz, P., Komaromi, I., Martin, R. L., Fox, D. J., Keith, T., Al-Laham, M. A., Peng, C. Y., Nanayakkara, A., Challacombe, M., Gill, P. M. W., Johnson, B., Chen, W., Wong, M. W., Gonzalez, C., and Pople, J. A. (2003) *Gaussian 03*, Rev. B. 04, Gaussian, Inc., Pittsburgh, PA

Structure of the PQQ Radical in Quinoproteins

42. Schaftenaar, G., and Noordik, J. H. (2000) *J. Comput. Aided Mol. Des.* **14**, 123–134
43. de Beer, R., van Ormondt, D., van Ast, M. A., Banen, R., Duine, J. A., and Frank, J. (1979) *J. Chem. Phys.* **70**, 4491–4495
44. Westerling, J., Frank, J., and Duine, J. A. (1979) *Biochem. Biophys. Res. Commun.* **87**, 719–724
45. de Jong, G. A., Geerlof, A., Stoorvogel, J., Jongejan, J. A., de Vries, S., and Duine, J. A. (1995) *Eur. J. Biochem.* **230**, 899–905
46. Kano, K., Mori, K., Uno, B., Kubota, T., Ikeda, T., and Senda, M. (1990) *Bioelectrochem. Bioenerg.* **24**, 193–201
47. de Beer, R., Duine, J. A., Frank, J., and Large, P. J. (1980) *Biochim. Biophys. Acta* **622**, 370–374
48. Jongejan, A., Jongejan, J. A., and Hagen, W. R. (2001) *J. Comput. Chem.* **22**, 1732–1749
49. Reddy, S. Y., and Bruce, T. C. (2004) *Proc. Natl. Acad. Sci. U. S. A.* **101**, 15887–15892
50. Mesecar, A. D., Stoddard, B. L., and Koshland, D. E., Jr. (1997) *Science* **277**, 202–206